RSC Advances

ROYAL SOCIETY OF CHEMISTRY

www.rsc.org/advances

Self-doped polyaniline/molybdenum oxide composite nanorods for supercapacitor

Li-Jun Bian, Hai-Long He, Xiao-Xia Liu*

Department of Chemistry, Northeastern University, Shenyang, 110819

Correspondence: xxliu@mail.neu.edu.cn, Fax: 86-24-83689510, Tel: 86-24-83689510

Abstract

A composite film of self-doped polyaniline and molybdenum oxide (SPAN/MoO_x) was prepared through multi-potential steps in which the working electrode was held at – 0.7 and 1.2 V alternately. The as-prepared composite was characterized by X-ray photoelectron spectroscopy (XPS) and fourier transformation infrared spectrophotometry (FTIR), its surface morphologies was investigated by scanning electron microscopy (SEM). Supercapacitive performance of the composite film was investigated by cyclic voltammetry, galvanostatic charge/discharge and electrochemical impedance spectroscopy (EIS). The SPAN/MoO_x displayed electroactivities in a large potential window from −0.8 to 1.0 V, showing the combination of SPAN and MoO_x's electroactivities in the composite. The SPAN/MoO_x displayed a specific capacitance of 570 $F\cdot g^{-1}$ at a current density of 1.7 $A\cdot g^{-1}$, which is higher than those of similar prepared SPAN (408 $F\cdot g^{-1}$) and MoO_x (100 $F\cdot g^{-1}$). The symmetric supercapacitor assembled by using SPAN/MoO_x as both of the electrodes showed good rate behavior with an energy density of 35 $Wh\cdot kg^{-1}$ at a high power density of 4.7 $kW\cdot kg^{-1}$.

Keywords: self-doped polyaniline, molybdenum oxide, supercapacitor

Introduction

Electrochemical capacitors, also known as supercapacitors, are promising energy storage devices because of their high power density and long cycle life[1]. However, the energy density of supercapacitor needs to be increased to meet the increasing energy demands. Increasing working voltage is a good way to enhance energy density E of supercapacitor as $E= 1/2CV^2$(C and V are specific capacitance and working voltage, respectively)[2]. The working voltage of a supercapacitor mainly depends on the charge storage potential window of its electrode materials. Incorporation pesudocapacitive materials with electroactivity in different potential ranges in one electrode can effectively increase its charge storage potential window[3, 4]. However, the development of pseudocapacitive materials which is electroactive in negative potential range is less explored. Molybdenum oxide (MoO_x) has attracted much attention in the field of energy storage owing to its low cost and high electrochemical activity in wide potential range[5, 6]. Nevertheless, its capacitive applications were impeded by the poor ionic and electronic conductivity of bulk MoO_x materials[6]. Combination of MoO_x with other capacitive materials was tried to improve its capacitive behaviors[7-13]. An intertwined composite of molybdenum trioxide nanowires and multiwall carbon nanotubes displayed superior capacitive charge storage properties to those of the oxide due to the improved electronic and ionic conductivities[9]. Conductive ZnO nanorods were used as supports for MoO_3 to improve its conductivity. The obtained ZnO@MoO_3 core/shell nanocable electrode displayed a specific capacitance of 236

$F \cdot g^{-1}$ at the scan rate of 5 $mV \cdot s^{-1}$, which is much larger than that of MoO_3 nanoparticles (~56 $F \cdot g^{-1}$)[10]. Charge storage properties of MoO_3 were also improved by polypyrrole coating due to the reduced internal resistance[11]. Coaxial heterostructure nanobelts of MoO_3 and polyaniline (PANI) prepared via in situ oxidative polymerization of aniline on surfaces of MoO_3 nanobelts displayed a high specific capacitance of 632 $F \cdot g^{-1}$ at a current density of $1A \cdot g^{-1}$ in the potential window of 0 ~ 0.6 V vs. SCE, due to the synergic effect between the PANI coating and the oxide core[13]. However, to the best of the authors' knowledge, there is no reported about using molybdenum oxide as composite component to enlarge charge storage potential window although its electroactivity in negative potential range endows it a good candidate to extend the negative potential limit.

In our previous work, self-doped PANI (SPAN) with enlarged charge storage potential window was prepared through incorporation of sulfonate group on the polymer chain[14]. In this work, MoO_x was incorporated in SPAN to further improve the capacitive properties in negative potentials (enlarge the potential window of the electrode material to −0.6 ~ 0.8 V vs. SCE). In addition, the counter ions (sulfonate groups) are covalently bounded in the polymer chain. Thus, fast charge/discharge kinetics can be achieved as during charge/discharge, only protons move out/into of the composite, leading to good rate capability for the composite[15]. The assembled symmetric supercapacitor by using the obtained SPAN/MoO_x composite as both of the electrode materials can work with a high operating voltage of 1.4 V and so display a high energy density of 37 $Wh \cdot kg^{-1}$ at a power density of 1 $kW \cdot kg^{-1}$. It can also work

at a high power density of 4.7 $kW \cdot kg^{-1}$ with only a slightly decreased energy density of 35 $Wh \cdot kg^{-1}$.

Experimental

2.1. *Materials and apparatus*

Aniline was distilled before use. Other chemicals were of analytical grade and used as received. Carbon cloth (C) obtained from SGL group (Germany) was used as working electrode for electrochemical deposition of SPAN/MoO_x composite, MoO_x and SPAN. The obtained composite was characterized by X-ray photoelectron spectroscopy (XPS) on a Multilab 2000 electron spectrometer (Thermo electron corporation, England). Fourier transform infrared spectrophotometer (FT-IR) (VERTEX70, Bruker Optics, Germany) was used to obtain FTIR spectra of SPAN, SPAN/MoO_x with KBr pellets. A scanning electron microscope (LEO SUPRA 35, Carl Zeiss, Germany) was used to investigate morphologies of the obtained electrodes.

2.2. *Electrochemical experiments*

Electrochemical experiments were performed in three-electrode electrochemical cell on a multi-channel electrochemical analyzer, VMP3 (Bio-Logic-Science Instruments, France). Platinum plate and saturated calomel electrode (SCE) were used as counter and reference electrodes, respectively. SPAN/MoO_x composite was electrodeposited from a solution of 0.1 M aniline, 0.05 M metanilic acid and 0.05 M Na_2MoO_4 by multi-potential steps in which the working electrode was held at –0.7

and 1.2 V, with a duration of 30 s for each step, alternately for 30 times. SPAN and MoO_x was similarly prepared for comparison. Electroactivities of the electrodes were studied using cyclic voltammetric scans in the potential range of –0.8 to 1.0 V in 0.5 M H_2SO_4. Constant current charge/discharge experiments were preformed in the potential range of –0.6 to 0.8 V to study their pseudocapacitive properties. Electrochemical impedance spectroscopy (EIS) measurements were conducted in the frequency range of 100 kHz to 100 mHz.

A symmetric supercapacitor (SPAN/MoO_x – SPAN/MoO_x) was assembled using SPAN/MoO_x as both of the anode and the cathode with a filter paper soaked with 0.5 M H_2SO_4 as separator.

Results and discussion

3.1 Materials characterization

Firstly, FT-IR was used to analyze the chemical component of SPAN/MoO_x. FTIR spectrum of similar prepared SPAN was also displayed for comparison (Fig. 1). Typical vibrations of PANI can be seen on both FTIR spectra. Stretching vibrations of C=C in quinoid and benzenoid rings appear at 1579 and 1507 cm^{-1}, respectively. The bands at 1390 and 1116 cm^{-1} are attribute to stretching vibrations of C–N of the secondary aromatic amine and of CN^+ in the polaron structure of PANI[16]. O=S=O and C–S stretching appear at 1402 and 620 cm^{-1}, respectively which can be ascribed to the sulfonate groups covalently bonded to the polymer chain[16]. The peak at 902 cm^{-1} in the spectrum of SPAN/MoO_x is associated with Mo-O[17], showing the successful

incorporation of MoO_x in SPAN.

Fig. 1

Fig. 2a shows the wide-survey XPS spectrum of SPAN/MoO_x composite, in which signals of C, N, O, Mo and S elements can be detected. The core level spectrum of Mo 3d peaks is shown in Fig. 2b, which can be deconvoluted into the doublets for Mo^{6+} at 232.9 and 235.9 eV, and Mo^{5+} at 231.7 and 234.8 eV, respectively. This indicates that the molybdenum exists in mixed valence in the composite. The N 1s broad band can be deconvoluted into three peaks (Fig. 2c) [18]. The peak at 398.3 and 399.8 eV can be assigned to the quinoid imine (=N–) and the benzenoid amine (–NH–), respectively. The cationic nitrogen atoms ($=NH^+$) is located at 401.6 eV. The ratio of ([=N] + [$=N^+$]) / [NH] is 0.99, indicating that SPAN is in the emeraldine state in the composite.

Fig. 2

Morphologies of SPAN, MoO_x and SPAN/MoO_x were investigated by SEM (Fig. 3). It can be seen that MoO_x exists in particles (Fig. 3a) while SPAN exists in irregular shapes (Fig. 3b) which should be due to the secondary polymer growth[19]. Nanorod composite can be seen in Fig. 3c, indicating that one-dimensional (1D) growth was directed through organic-inorganic incorporation. The MoO_x in the composite with reduced molybdenum oxidation state can exist in the form of $MoO_{3-x}(OH)_x$[17]. Then hydrogen bonding can be formed between SPAN and MoO_x during the organic-inorganic incorporation, which can inhibit the secondary polymer

growth which is advantageous to the 1D growth[20]. The micro-porous structure fabricated by SPAN/MoO_x nanorod with high specific area facilitates effective contacts between electrode materials and electrolyte. Short ion transportation path can be established as well, which will lead to fast charge/discharge rate.

Fig. 3

3.2. Capacitive performance of SPAN/MoO_x composite film

Electrochemical behavior of SPAN/MoO_x was studied by cyclic voltammetry in 0.5 M H_2SO_4 solution. The cyclic voltammogram (CV) of SPAN/MoO_x together with those of SPAN and MoO_x are shown in Fig. 4. Typical redox pairs of PANI can be seen on both CVs of SPAN and SPAN/MoO_x. The redox pairs I_a/ I_c and II_a/ II_c on the CV of SPAN/MoO_x, as well as I'_a/I'_c and II'_a/II'_c on the CV of SPAN, are corresponding to emeraldine/pernigraniline and leucoemeraldine/emeraldine exchange of PANI[21]. Compare to I'_a which corresponding to the oxidation of emeraldine state of PANI in SPAN to its pernigraniline state (scheme 1)[22], the potential of I_a positively shifts for the emeraldine/pernigraniline exchange of the polymer in the composite. This should be related to the increased acidity in the composite film due to the incorporation of MoO_x which may exist in the form of $MoO_{3-x}(OH)_x$[17]. The potential of II_a doesn't display positive shift compare to II'_a as the leucoemeraldine/emeraldine exchange is insensitive to acidity (scheme 2)[22]. Instead, II_a displays slightly negative shift compare to II'_a, which may be due to the improved electronic conductivity of the composite, supported by the EIS results (see

below for details). Redox peaks I''_a/I''_c, II''_a/II''_c and III''_a/III''_c on the CV of MoO_x correspond to the reversible oxidation/reduction of oxide and the corresponding intercalation/deintercalation of H^+ into/out of the MoO_x which contribute pseudocapacitance for it[23, 24]. Similar redox pairs can also be observed on the CV of SPAN/MoO_x although some overlap with those of PANI, showing successful incorporation of MoO_x into SPAN. It can be seen from Fig. 4 that SPAN/MoO_x displays higher electroactivities than SPAN and MoO_x due to the combined electroactivity and its micro-porous structure fabricated by composite nanorods (Fig. 3c).

scheme 1

scheme 2

Fig.4

Galvanostatic charge/discharge experiments were conducted on SPAN/MoO_x, SPAN and MoO_x to investigate their charge storage properties (Fig.5). SPAN/MoO_x shows improved charge storage property in the negative potentials due to the incorporation of MoO_x (inset of Fig. 5). To further investigate the charge/discharge potential window of SPAN/MoO_x, galvanostatic charge/discharge experiments were conducted on the composite at different voltages at a fixed current density of 1.7 A g^{-1} (Fig. 6). The charge/discharge curves approximately follow the same trace for charging, suggesting that the stable charge/discharge potential window of SPAN/MoO_x could be extended to 1.4 V from – 0.6 to 0.8 V which is helpful for its energy density increment. SPAN/MoO_x composite shows longer charge/discharge

duration than SPAN and MoO_x (Fig. 5), again indicating its better charge storage performance. The specific capacitance of the materials (C_s) can be calculated from the discharge curve according to Eq. (3-1)

$$C_s = \frac{it}{m\Delta V} \qquad (3\text{-}1)$$

where i and t are discharge current and time, respectively. The ΔV is the discharge potential range, m is the mass of the active material. Based on the charge/discharge experiments, SPAN/MoO_x displays a specific capacitance of 570 $F \cdot g^{-1}$ which is higher than that of SPAN (408 $F \cdot g^{-1}$) and MoO_x (100 $F \cdot g^{-1}$).

Fig. 5

Fig. 6

Electrochemical impedance characteristics of SPAN, MoO_x and SPAN/MoO_x were investigated at open circuit potential in the frequency range from 100 kHz to 100 mHz. The Nyquist plots are shown in Fig. 7. All of the electrodes show impedance arc in the high frequency region and straight line in the low frequency region, which is typical for capacitive materials. SPAN/MoO_x displays lower combined series resistance (R_s) than SPAN and MoO_x, calculated from the crossing of the high-frequency domain end and the real component axis, suggesting that it has improved electrical conductivity.

Fig. 7

3.3 *Application in model capacitors*

To investigate the performance of SPAN/MoO_x in capacitor, a symmetric supercapacitor, SPAN/MoO_x – SPAN/MoO_x was fabricated by using 0.5 M H_2SO_4 as electrolyte and SPAN/MoO_x as both of the anode and cathode.

CV measurements were conducted on SPAN/MoO_x – SPAN/MoO_x capacitor at various scan rates from 0 to 1.4 V (Fig. 8). Distorted rectangular CV curves can be seen in Fig. 8, indicating the pseudocapacitive behavior of the capacitor. The peak current on the CVs increases with increasing scan rate, suggesting its high reversibility for fast charge/discharge response.

Fig. 8

Fig. 9

Fig. 9 shows the constant current charge/discharge curves of the symmetric supercapacitor collected at the current densities from 0.8 to 4.2 $A \cdot g^{-1}$. The charge/discharge curves are nearly symmetric, indicating its good reversibility with the operating voltage of 1.4 V. The specific capacitance of the capacitor can be calculated by Eq.(3-2) where m is the mass of active materials on both of the two electrodes, V is the operating voltage, i and t are discharge current and time, respectively. SPAN/MoO_x – SPAN/MoO_x capacitor displays a specific capacitance of 130 $F \cdot g^{-1}$ at the current density of 1.3 $A \cdot g^{-1}$. The energy density E and power density P of the symmetric capacitor can be calculated by Eq. (3-3), (3-4)[3]

$$C = \frac{it}{mV} \qquad (3\text{-}2)$$

$$E = \frac{1}{2}CV^2 \qquad (3\text{-}3)$$

$$P = E / t \qquad (3\text{-}4)$$

where C is the specific capacitance of the capacitor, V is the operating voltage and t is the discharge time obtained by chronopotentiometry. The results were summarized in Fig. 10. The SPAN/MoO_x – SPAN/MoO_x capacitor displays a high energy density of 37 $Wh \cdot kg^{-1}$ at the power density of 1 $kW \cdot kg^{-1}$ which is higher than those of other reported supercapacitors assembled by molybdenum oxide based electrode materials, such as (+)α-MoO_3//AC(-) (16.72 $Wh \cdot kg^{-1}$ at 325 $W \cdot kg^{-1}$)[25], (+)AC//PPy@MoO_3(-) (20 $Wh \cdot kg^{-1}$ at 75 $W \cdot kg^{-1}$)[12], (+)MoO_3/MWCNTs//MoO_3/MWCNTs(-) (7.28 $Wh \cdot kg^{-1}$ at 672 $W \cdot kg^{-1}$)[26]. Moreover, the capacitor only displays a very slightly decrease in its energy density (to 35 $Wh \cdot kg^{-1}$) when the power density increases to 4.7 $kW \cdot kg^{-1}$, showing its super rate capability. This can be attributed to the increased electronic conductivity as well as the improved ionic conductivity of the electrode material and so the facilitated redox reactions for charge storage, revealing that SPAN/MoO_x features good performance as pesudocapacitive materials.

Fig. 10

Charge/discharge cycling performance of the SPAN/MoO_x – SPAN/MoO_x capacitor was investigate with an operating voltage of 1.4 V at a current density of 1.7 $A \cdot g^{-1}$ for 1000 cycles (Fig. 11). A capacitance decrease can be seen in the first 100 cycles which may be due to the fall off of those of the electroactive materials loosely attached on the electrode surfaces. Then the underlying material have chance to sufficiently contact with the electrolyte, resulting in capacitance increase in the following 300 cycles. After 1000 charge-discharge cycles, the capacitor retains 91%

of it's activited capacitance (the capacitance at 400th cycle) and 77% of its initial capacitance (the capacitance in the first cycle), showing improved stability than our SPAN based supercapacitor[16].

Fig.11

Conclusion

SPAN/MoO_x composite film was synthesized through electro-codeposition of MoO_x and SPAN, directing to one-dimensional growth of SPAN. Due to the combined electroactivity and organic-inorganic synergistic effects, SPAN/MoO_x shows electroactivity in a wide potential range of 1.4 V from – 0.6 to 0.8 V vs. SCE and improved pesudocapacitive behaviors. The assembled symmetric supercapacitor SPAN/MoO_x – SPAN/MoO_x can work with an operating voltage of 1.4 V and so displays a high energy density of 37 $Wh{\cdot}kg^{-1}$ at the power density of 1 $kW{\cdot}kg^{-1}$. At a high power density of 4.7 $kW{\cdot}kg^{-1}$, its energy density is still as high as 35 $Wh{\cdot}kg^{-1}$, demonstrating its super rate capability.

Acknowledgements

We gratefully acknowledges financial supports from Fundamental Research Funds for the Central Universities of China (N140503002), the National Natural Science Foundation of China (21273029) and Research Foundation for Doctoral Program of Higher Education of China (20120042110024).

References

1. B. E. Conway, *J. Electrochem. Soc.*, 1991, **138**, 1539.
2. K. H. An, W. S. Kim, Y. S. Park, J. M. Moon, D. J. Bae, S. C. Lim, Y. S. Lee and Y. H. Lee, *Adv. Funct. Mater.*, 2001, **11**, 387-392.
3. W. F. Mak, G. Wee, V. Aravindan, N. Gupta, S. G. Mhaisalkar and S. Madhavi, *J. Electrochem. Soc.*, 2012, **159**, A1481-A1488.
4. W. Wang, W. Liu, Y. Zeng, Y. Han, M. Yu, X. Lu and Y. Tong, *Adv. Mater.*, 2015, **27**, 3572-3578.
5. I. Shakir, M. Shahid, U. A. Rana and M. F. Warsi, *RSC Adv.*, 2014, **4**, 8741-8745.
6. D. Guan, X. Gao, J. Li and C. Yuan, *Appl. Surf. Sci.*, 2014, **300**, 165-170.
7. Q. Mahmood, H. J. Yun, W. S. Kim and H. S. Park, *J. Power Sources*, 2013, **235**, 187-192.
8. T. Tao, Q. Chen, H. Hu and Y. Chen, *Mater. Lett.*, 2012, **66**, 102-105.
9. I. Shakir and M. Sarfraz, *Electrochim. Acta*, 2014, **147**, 380-384.
10. G.-R. Li, Z.-L. Wang, F.-L. Zheng, Y.-N. Ou and Y.-X. Tong, *J. Mater. Chem.*, 2011, **21**, 4217.
11. X. Zhang, X. Zeng, M. Yang and Y. Qi, *ACS Appl Mater Interfaces*, 2014, **6**, 1125-1130.
12. Y. Liu, B. Zhang, Y. Yang, Z. Chang, Z. Wen and Y. Wu, *J.Mater.Chem.A*, 2013, **1**, 13582-13587.
13. F. Jiang, W. Li, R. Zou, Q. Liu, K. Xu, L. An and J. Hu, *Nano Energy*, 2014, **7**, 72-79.
14. L.-J. Bian, F. Luan, S.-S. Liu and X.-X. Liu, *Electrochim. Acta*, 2012, **64**, 17-22.
15. J. Yue, Z. H. Wang, K. R. Cromack, A. J. Epstein and A. G. MacDiarmid, *J. Am. Chem. Soc.*, 1991, **113**, 2665-2671.
16. L.-J. Bian, F. Luan, S.-S. Liu and X.-X. Liu, *Electrochim. Acta*, 2012, **64**, 17-22.
17. L.-J. Bian, J.-H. Zhang, J. Qi, X.-X. Liu, D. Dermot and K.-T. Lau, *Sen. Actuators B.*, 2010, **147**, 73-77.
18. B.-X. Zou, Y. Liang, X.-X. Liu, D. Diamond and K.-T. Lau, *J. Power Sources*, 2011, **196**, 4842-4848.
19. J. X. Huang and R. B. Kaner, *Chem. Commun.*, 2006, 367-376.
20. X.-X. Liu, Y.-Q. Dou, J. Wu and X.-Y. Peng, *Electrochim. Acta*, 2008, **53**, 4693-4698.
21. Z. Wang, L. Jiao, T. You, L. Niu, S. Dong and A. Ivaska, *Electrochem. Commun.*, 2005, **7**, 875-878.
22. X.-X. Liu, L.-J. Bian, L. Zhang and L.-J. Zhang, *J. Solid State Electrochem.*, 2007, **11**, 1279-1286.
23. W. Tang, L. Liu, S. Tian, L. Li, Y. Yue, Y. Wu and K. Zhu, *Chem. Commun.*, 2011, **47**, 10058-10060.
24. T. Brezesinski, J. Wang, S. H. Tolbert and B. Dunn, *Nat. Mater.*, 2010, **9**, 146-151.
25. F. Barzegar, A. Bello, D. Y. Momodu, J. K. Dangbegnon, F. Taghizadeh, M. J. Madito, T. M. Masikhwa and N. Manyala, *RSC Adv.*, 2015, **5**, 37462-37468.
26. L. S. Aravinda, U. Bhat and B. Ramachandra Bhat, *Electrochim. Acta*, 2013, **112**, 663-669.

Figure legends and scheme caption

Fig.1 FTIR spectra of SPAN and SPAN/MoO_x.

Fig.2 XPS survey spectrum of SPAN/MoO_x (a), Mo 3d (b) and N 1s (c) core level XPS spectra.

Fig.3 SEM images of MoO_x (a), SPAN (b) and SPAN/MoO_x(c).

Fig.4 Cyclic voltammograms of SPAN, SPAN/MoO_x and MoO_x in 0.5 M H_2SO_4 (scan rate: 50 mV s^{-1}).

Fig.5 Galvanostatic charge/discharge curves of SPAN, SPAN/MoO_x and MoO_x at 1.7 A g^{-1}. Inset shows the discharge curves of the three electrode.

Fig.6 Galvanostatic charge/discharge curves of SPAN/MoO_x collected at different voltages at a fixed current density of 1.7 A g^{-1}.

Fig.7 Nyquist plots of SPAN, SPAN/MoO_x and MoO_x films collected in the range of 100 mHz to 100 kHz in 0.5 M H_2SO_4 at open circuit potential. Inset shows the Nyquist plots of SPAN and MoO_x films, respectively.

Fig.8 CV profiles of SPAN/MoO_x-SPAN/MoO_x capacitor at various scan rates.

Fig.9 Galvanostatic charge/discharge curves of SPAN/MoO_x-SPAN/MoO_x capacitors at different current density.

Fig.10 Ragone plots of SPAN/MoO_x-SPAN/MoO_x capacitor

Fig.11 Cycling stability of SPAN/MoO_x-SPAN/MoO_x collected by galvanostatic charge/discharge experiments at a current density of 1.7 A·g^{-1}.

Scheme 1 Exchange between the emeraldine and the pernigraniline states of PANI

Scheme 2 Exchange between the leucoemeraldine and the emeraldine states of PANI

Figure 1

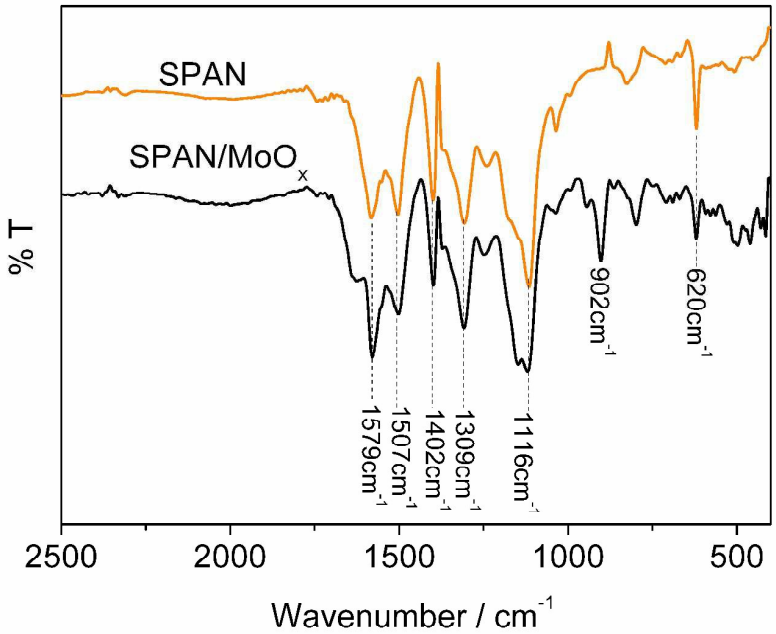

Figure 2

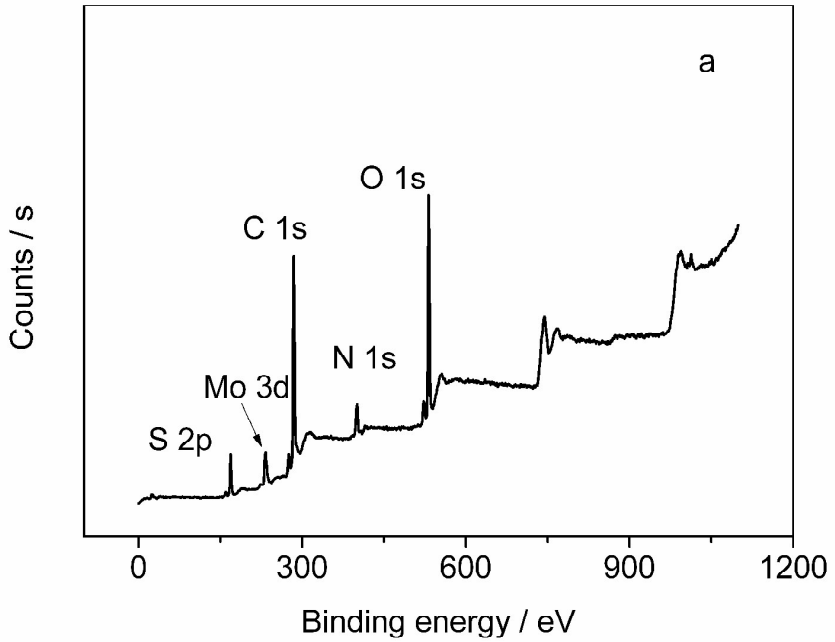

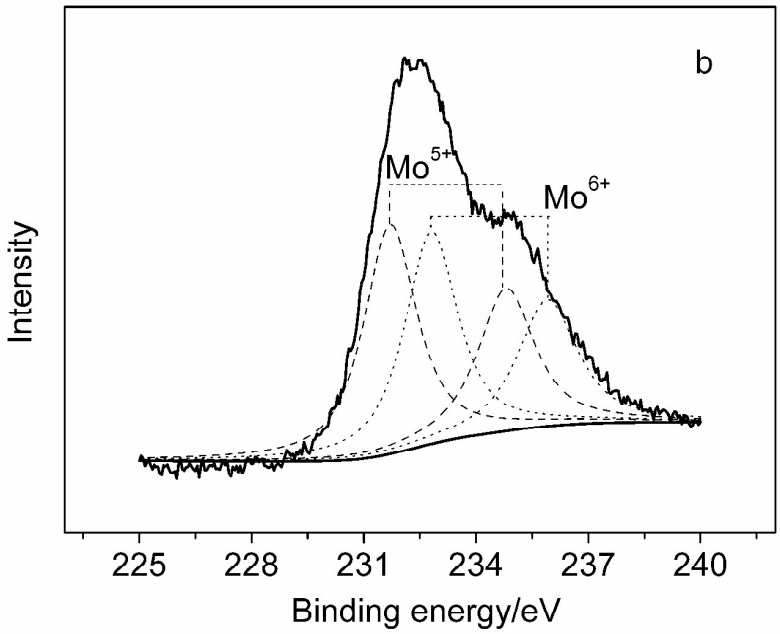

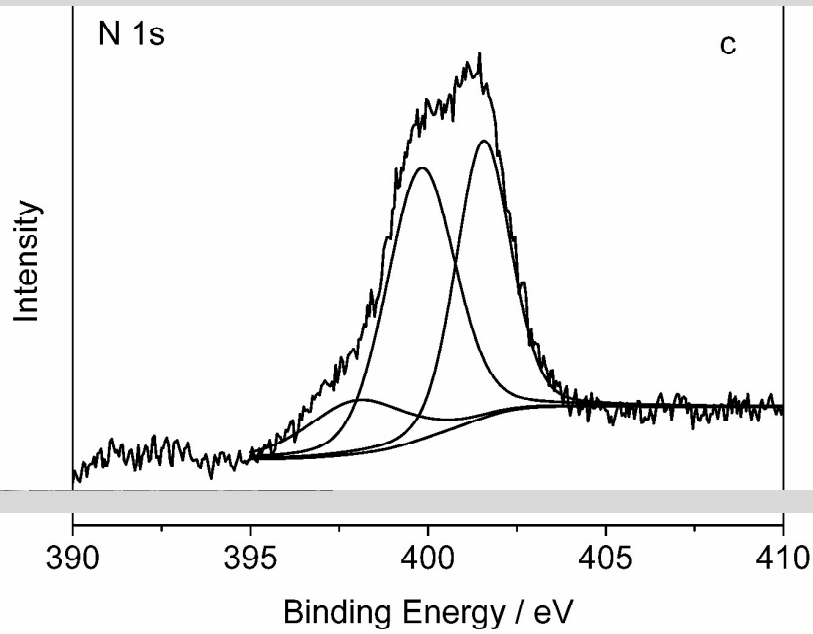

Figure 3

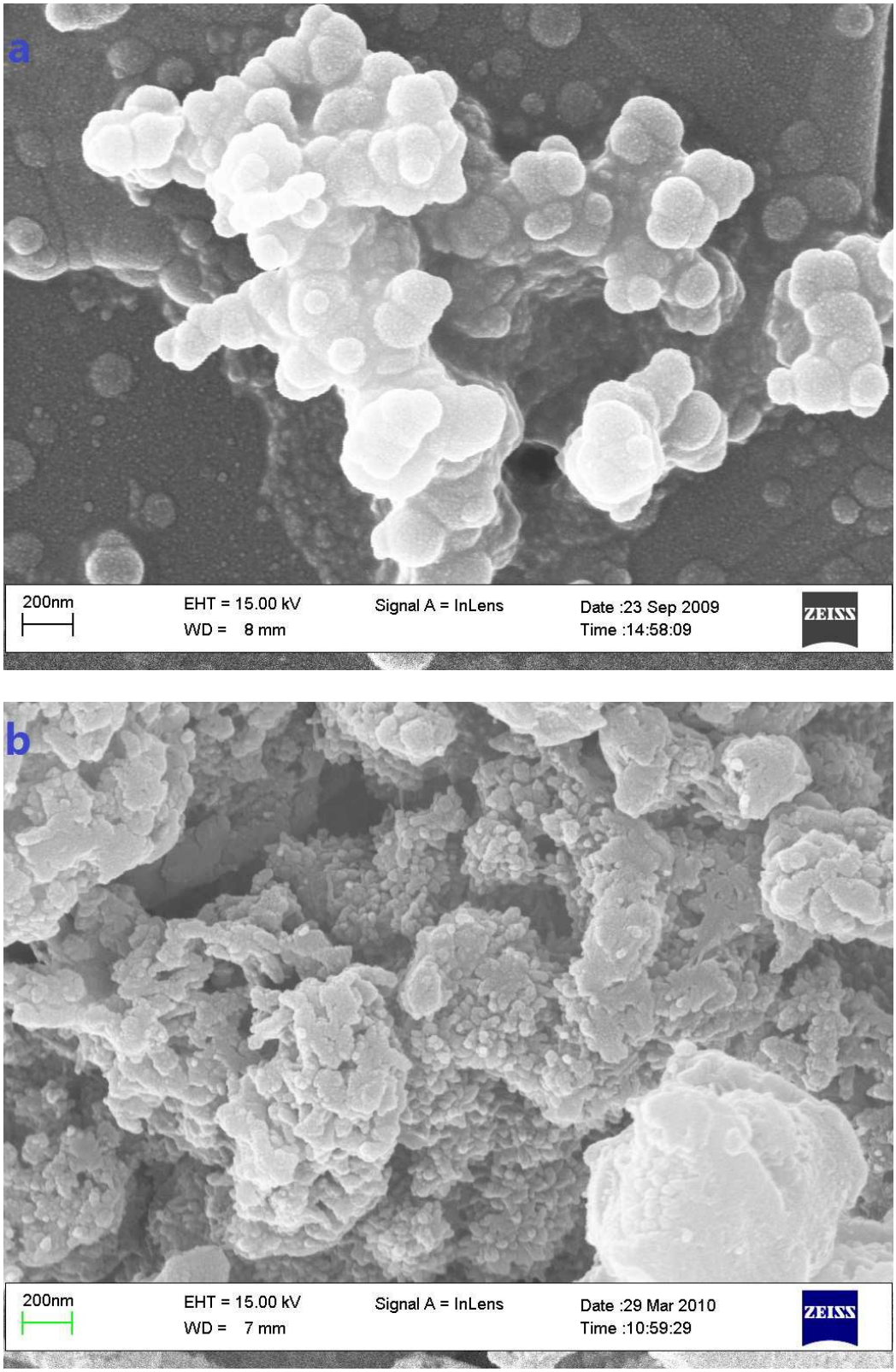

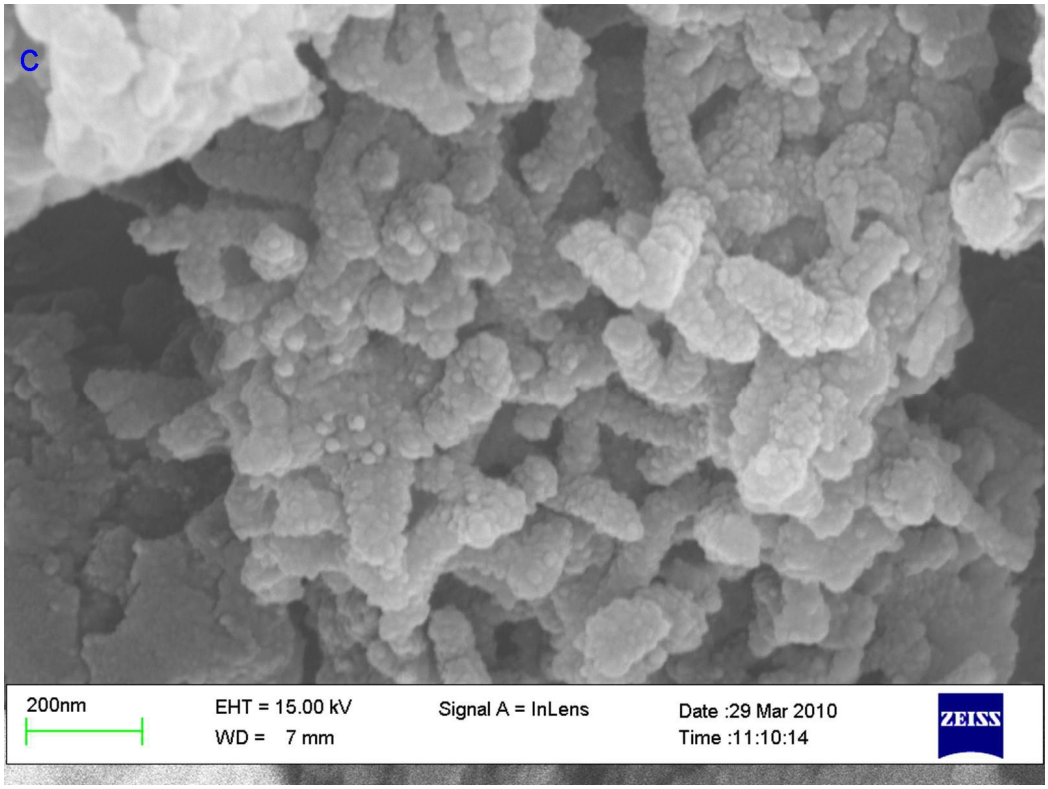

Figure 4

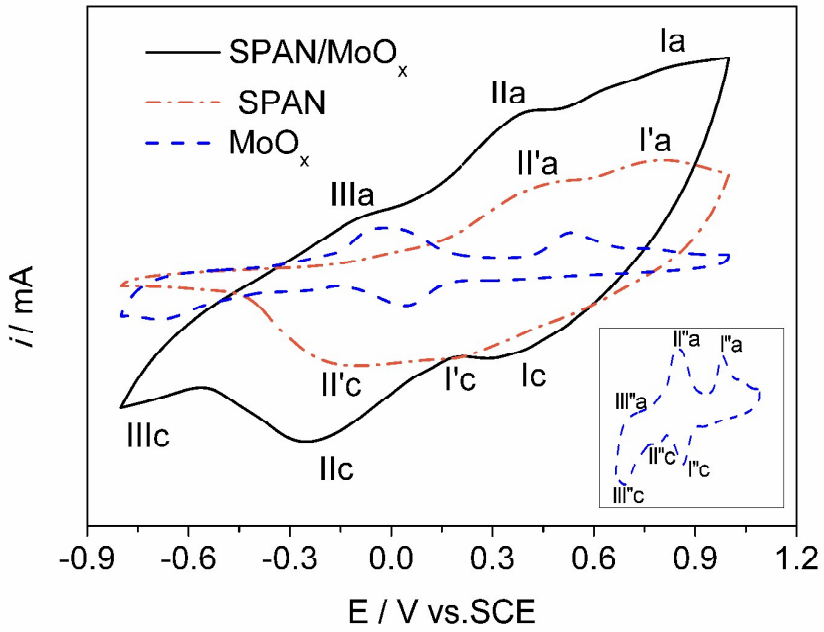

Figure 5

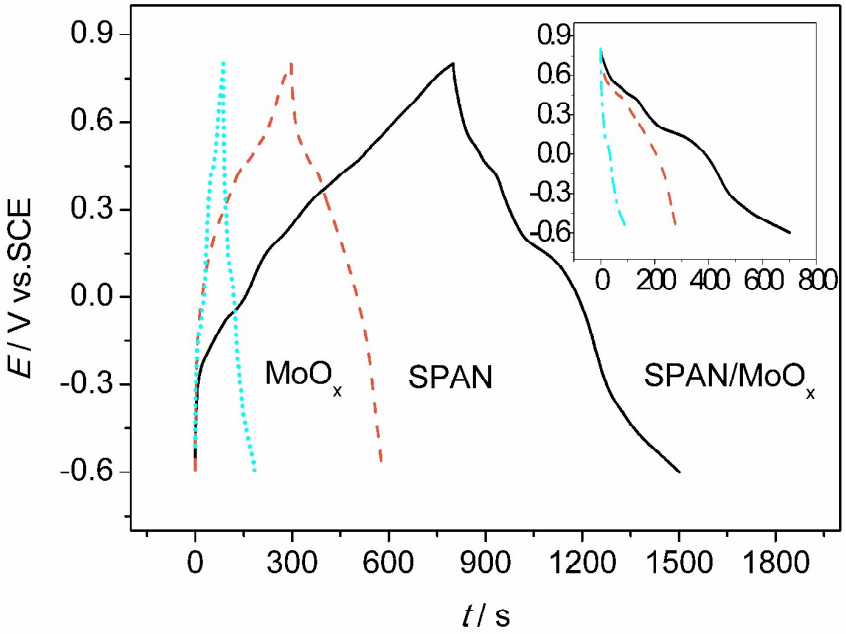

Figure 6

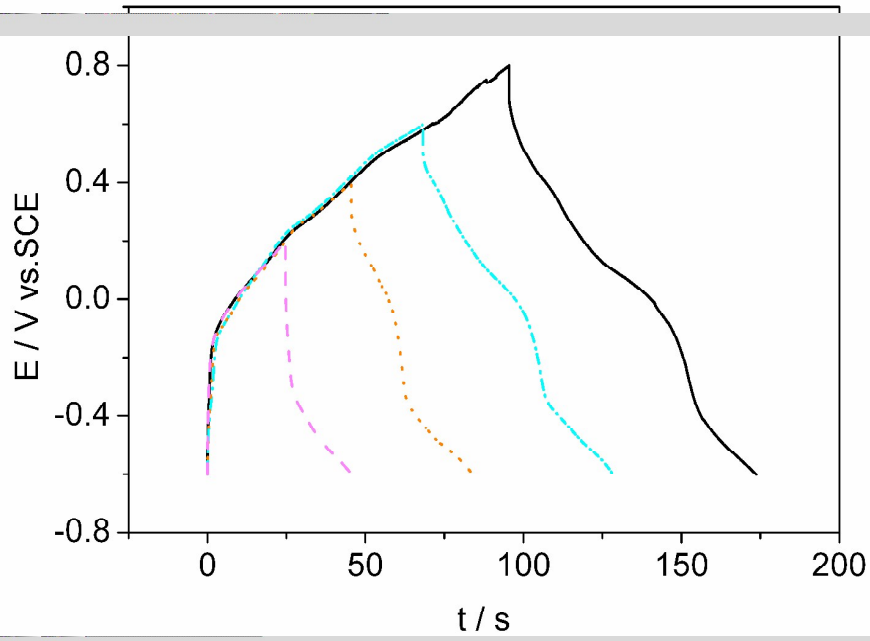

Figure 7

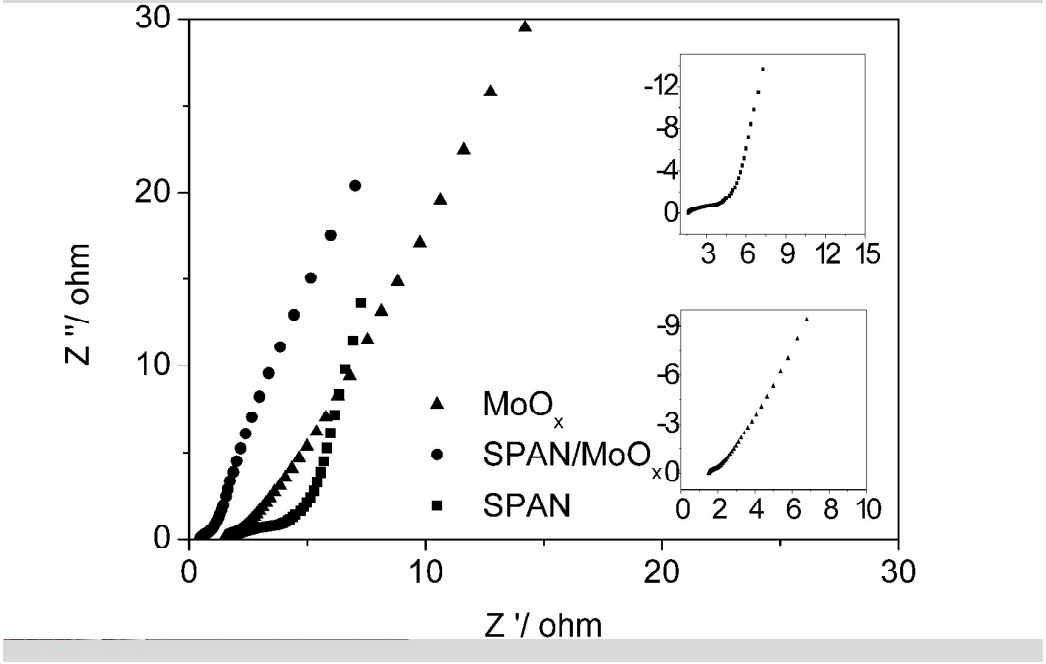

Figure 8

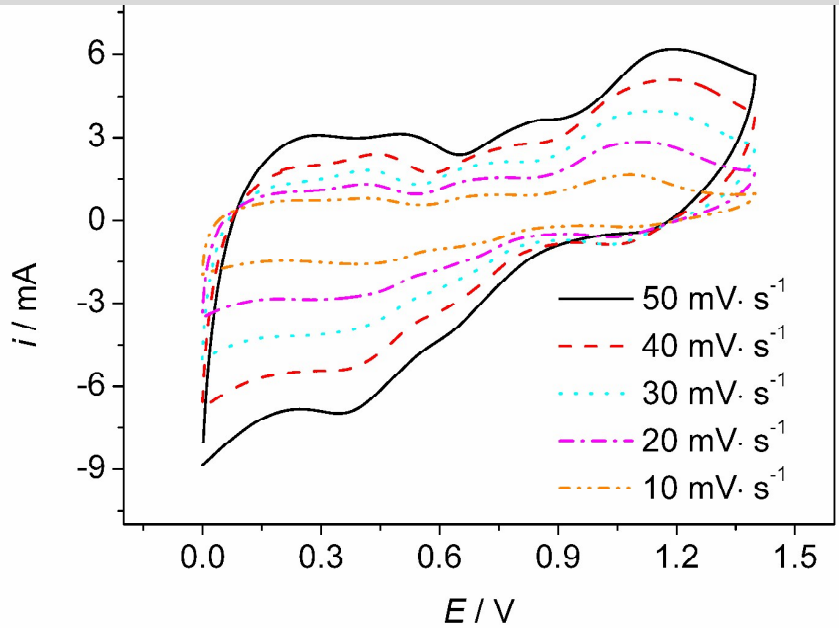

Figure 9

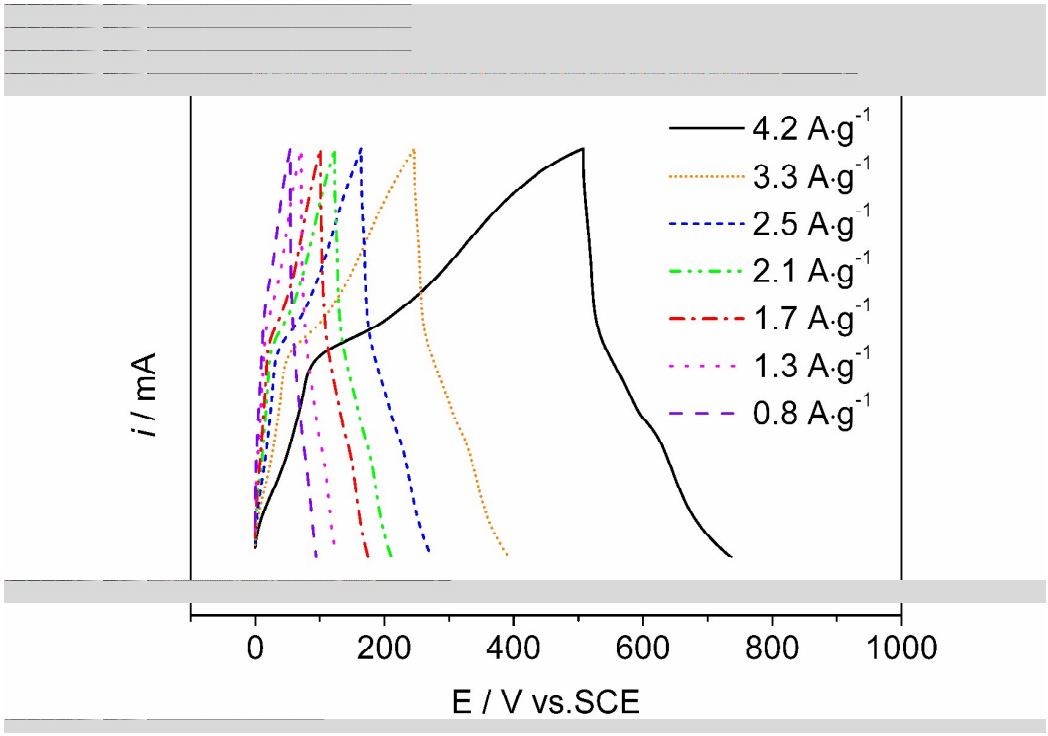

Figure 10

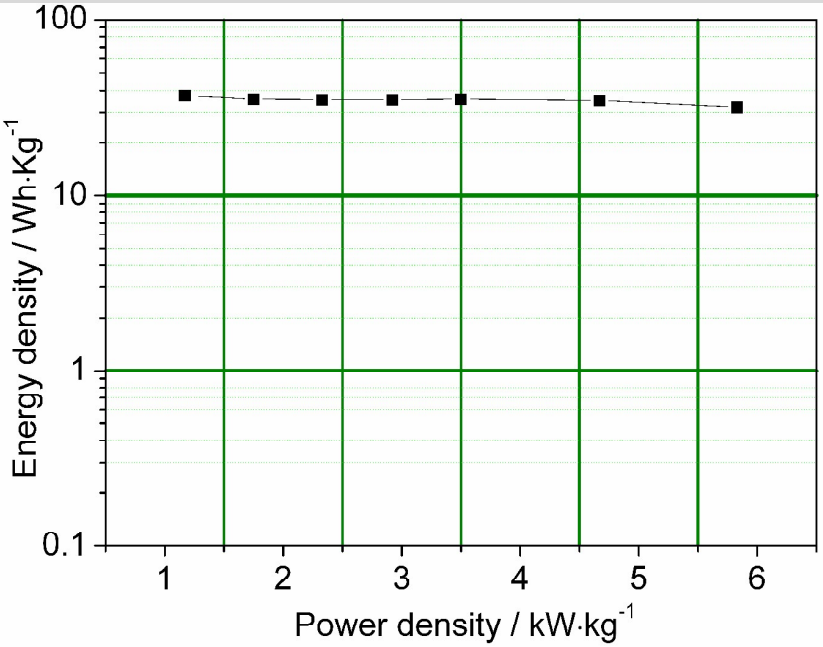

Figure 11

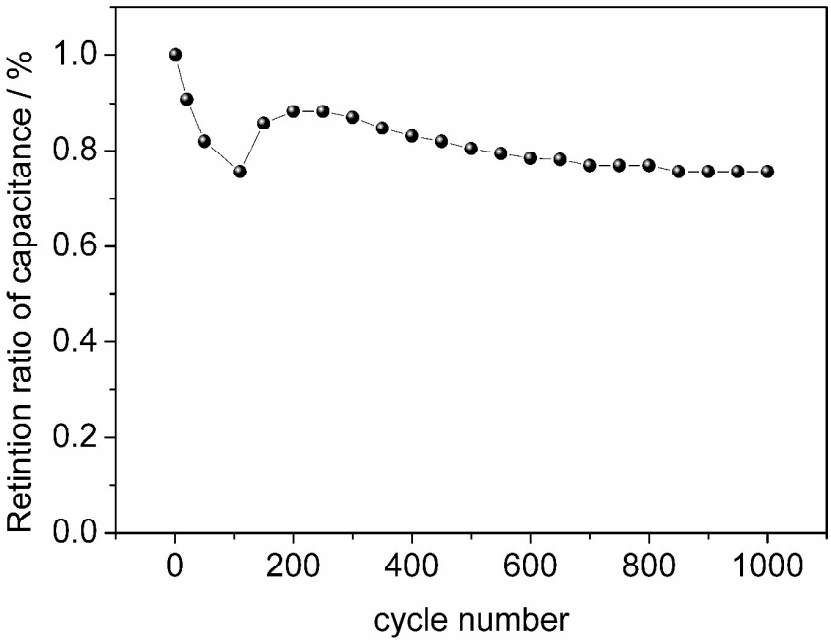

Scheme 1

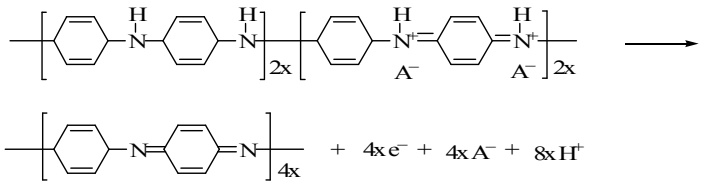

Scheme 2